Computational and Applied Mathematics (2026) 45:181
https://doi.org/10.1007/s40314-025-03577-1

Impact of reynolds number and slip/no-slip boundary condition on stratification in a two-dimensional boussinesq system

Edom Belayneh[1] · Xiaobai Chen[2] · Ruthwik Nadam[2] · Jiahong Wu[3] · Xiaoming Zheng[4]

Received: 15 September 2025 / Revised: 2 December 2025 / Accepted: 4 December 2025

Abstract

Buoyancy-driven fluid flows, such as tornadoes, hurricanes, and Rayleigh-Bénard convection (e.g., boiling water), exhibit a fundamental feature known as stratification: hotter (lighter) fluid rises while colder (heavier) fluid sinks. This process is described by the Boussinesq equations. Motivated by real-world applications, this paper explores via the Boussinesq equations how stratification is influenced by the Reynolds number and different boundary conditions (slip and no-slip). It is well known that the dynamics of fluids with no-slip boundary conditions is still not well understood in the high Reynolds number regime. First, we rigorously establish the large Reynolds number limit of viscous Boussinesq flow with an explicit convergence rate under the stress-free boundary condition. Second, we present a linear stability analysis for perturbations near the hydrostatic equilibrium, the stationary eventual temperature profile. Third, numerical simulations reveal the stratification is faster under the higher Reynolds numbers and the slip boundary condition. In particular, we observe the boundary plume eruptions that facilitate stratification and the seesaw-like oscillations for the large Reynolds numbers.

✉ Jiahong Wu
jwu29@nd.edu

✉ Xiaoming Zheng
zheng1x@cmich.edu

Edom Belayneh
belay1ey@cmich.edu

Xiaobai Chen
chen12x@cmich.edu

Ruthwik Nadam
nadam1r@cmich.edu

1 Department of Computer Science, C, Mount Pleasant, Mount Pleasant, MI 48858, USA

2 Department of Statistics, Actuarial & Data Science, Central Michigan University, Mount Pleasant, MI 48858, USA

3 Department of Mathematics, University of Notre Dame, Notre Dame, IN 46556, USA

4 Department of Mathematics, Central Michigan University, Mount Pleasant, MI 48858, USA

Published online: 22 December 2025

Keywords Boussinesq equations · Large Reynolds number limit · Hydrostatic stability · Boundary plume eruption · Seesaw oscillations

Mathematics Subject Classification 35Q35 · 76D05 · 65N30

1 Introduction

This paper combines rigorous analysis with numerical simulations to understand some crucial behaviors of buoyancy-driven fluids. These types of fluids are very common in our daily lives. Tornadoes, hurricanes, and Rayleigh-Bénard convection (such as boiling a pot of water) are notable examples of buoyancy-driven fluids.

One of the most significant features of buoyancy-driven fluids is the process of stratification. It occurs when fluid layers are arranged in a stable temperature gradient, often with colder (heavier) fluid below hotter (lighter) fluid. In many real-world applications, it is crucial to understand how the Reynolds number and different boundary conditions affect this process (see, e.g., Bartello and Tobias (2013); de Bruyn Kops (2015); Laval et al. (2003); Zhou and Diamessis (2016)). We perform extensive numerical simulations to study stratification behavior over a wide range of Reynolds numbers and under two types of boundary conditions: the slip boundary condition (or stress-free boundary condition) and the standard no-slip boundary condition. The simulations yield insightful results. For very large Reynolds numbers, fluids with no-slip boundary conditions are not well understood. Our simulations reveal an intriguing seesaw rotation behavior. In the case of stress-free boundaries, we are able to establish a rigorous large-Reynolds-number limit result.

Buoyancy-driven fluids stratify and converge to hydrostatic equilibrium. A natural question concerns the stability of perturbations near hydrostatic equilibrium. Hydrostatic equilibrium refers to the balance between gravity and pressure in a fluid or solid, occurring when the upward pressure force and the downward gravitational force balance each other out. This concept is fundamental in fluid mechanics, meteorology, and astronomy. In fact, our atmosphere is largely in hydrostatic equilibrium. Many books on geophysical fluid dynamics dedicate entire sections or even full chapters to this topic (see, e.g., Holton and Hakim (2012); Pedlosky (1987); Salmon (1998); Vallis (2017)).

In a joint work by two of the authors with C. Doering and K. Zhao, hydrostatic equilibrium given by a linear temperature profile was studied both theoretically and numerically. Doering et al. (2018) has provided valuable insights into the stability of perturbations and their large-time behavior. In the modeling of real geophysical fluids, however, the temperature profile is not necessarily a simple linear function of x_2 such as αx_2. Therefore, it is essential to investigate the stability of a more general hydrostatic equilibrium. This is a nontrivial problem, as stability properties can vary significantly depending on the temperature distribution. It remains a challenging open question, and to our knowledge, no rigorous results currently exist on this subject. This work presents a rigorous result on the linear stability near a general temperature profile.

1.1 Boussinesq system and stratification

We now make the above descriptions more precise in terms of the mathematical model for buoyancy-driven fluids, the Boussinesq equations. Our focus will be on the two-dimensional

Boussinesq system with velocity dissipation and no thermal diffusion,

$$\begin{cases} \partial_t \mathbf{u} + \mathbf{u} \cdot \nabla \mathbf{u} = -\nabla p + \nu \Delta \mathbf{u} + \theta \mathbf{e}_2, & x \in \Omega, t > 0, \\ \partial_t \theta + \mathbf{u} \cdot \nabla \theta = 0, \\ \nabla \cdot \mathbf{u} = 0, \end{cases} \tag{1.1}$$

where $\mathbf{x} = (x_1, x_2)$, $t > 0$, $\mathbf{u} = (u_1, u_2)$ is the velocity, p is pressure, θ is temperature, ν is kinematic viscosity, and $\mathbf{e_2} = (0, 1)$ is the unit vector. The spatial domain Ω is taken as the unit square, namely $\Omega = (-1, 1)^2$. To broaden the applicability of our rigorous analysis, our theorems actually apply to more general bounded domains with sufficiently smooth boundaries, except at a finite number of points where the corner angle is no greater than $\frac{\pi}{2}$. More details on this type of domain can be found in Doering et al. (2018).

The Boussinesq system (1.1) is supplemented with two different boundary conditions. The first is the no-slip boundary condition:

$$\mathbf{u}|_{\partial\Omega} = \mathbf{0},$$

and the second is the slip boundary condition (or stress-free boundary condition):

$$\mathbf{u} \cdot \mathbf{n} = 0, \qquad \omega = \partial_1 u_2 - \partial_2 u_1 = 0 \quad \text{on } \partial\Omega,$$

where $\mathbf{n}$ is the unit outward normal vector on the boundary $\partial\Omega$.

The first equation in (1.1) is simply the 2D Navier-Stokes equation with the forcing term $\theta\mathbf{e}_2$. This term represents buoyancy, which drives hotter (and therefore lighter) fluids upward and colder (heavier) fluids downward. The second equation in (1.1) states that the temperature is transported by the velocity field. A fundamental issue is to understand the evolution of temperature and provide a precise description of the final buoyancy distribution for general initial conditions. Our previous work (Doering et al. 2018) and (Tao et al. 2020) conducted a preliminary study of this problem and predicted that the temperature field converges to a stratified state $S(x_2)$. In a rectangular domain of width W, we define a height function of the initial temperature field θ_0 as

$$h(a) = \frac{1}{W} \text{area} \left\{(x_1, x_2) \in \Omega : \theta_0(x_1, x_2) \le a\right\}, \tag{1.2}$$

then the stratified state is the inverse function of h, that is ,

$$S(x_2) = h^{-1}(x_2). \tag{1.3}$$

As is well known, when the no-slip boundary condition is imposed, vorticity is generated at the boundary, and the large Reynolds number limit of fluid flows remains poorly understood. As demonstrated by the plots in Sect. 4, mushroom vortex structures form at the boundary. While this phenomenon has been extensively investigated theoretically and significant progress has been made, the limiting behavior of the Navier-Stokes solutions as the Reynolds number approaches infinity has not been completely resolved (see, e.g., (Bona and Wu 2002; Constantin et al. 2015, 2017; Constantin and Wu 1995; Gie et al. 2019; Kukavica et al. 2020, 2022; Lacave and Mazzucato 2016)). Numerical simulations serve as an indispensable tool in studying this limit. The numerical results presented in Section 4 provide valuable insight into the behavior of large-Reynolds-number Boussinesq flows under the no-slip boundary condition.

1.2 Main result of inviscid limit with slip boundary condition

However, when the slip boundary condition (or stress-free boundary condition) is imposed, we can rigorously show that the solution of the viscous Boussinesq equations converges to the corresponding solution of the inviscid Boussinesq equations as the Reynolds number approaches infinity. More precisely, if $(\mathbf{u}^{(\nu)}, \theta^{(\nu)})$ solves the following initial and boundary-value problem on the Boussinesq equations

$$\begin{cases} \partial_t \mathbf{u}^{(\nu)} + \mathbf{u}^{(\nu)} \cdot \nabla \mathbf{u}^{(\nu)} = -\nabla p^{(\nu)} + \nu \Delta \mathbf{u}^{(\nu)} + \theta^{(\nu)} \mathbf{e}_2, \quad x \in \Omega, t > 0, \\ \partial_t \theta^{(\nu)} + \mathbf{u}^{(\nu)} \cdot \nabla \theta^{(\nu)} = 0, \\ \nabla \cdot \mathbf{u}^{(\nu)} = 0, \\ \mathbf{u}^{(\nu)} \cdot \mathbf{n}|_{\partial\Omega} = 0, \quad \omega^{(\nu)}|_{\partial\Omega} = 0, \end{cases} \tag{1.4}$$

then, as the Reynolds number $Re := \nu^{-1} \to \infty$, the solution $(\mathbf{u}^{(\nu)}, \theta^{(\nu)})$, converges to the corresponding solution $(\mathbf{u}^{(0)}, \theta^{(0)})$ of its inviscid counterpart,

$$\begin{cases} \partial_t \mathbf{u}^{(0)} + \mathbf{u}^{(0)} \cdot \nabla \mathbf{u}^{(0)} = -\nabla p^{(0)} + \theta^{(0)} \mathbf{e}_2, \quad x \in \Omega, t > 0, \\ \partial_t \theta^{(0)} + \mathbf{u}^{(0)} \cdot \nabla \theta^{(0)} = 0, \\ \nabla \cdot \mathbf{u}^{(0)} = 0, \\ \mathbf{u}^{(0)} \cdot \mathbf{n}|_{\partial\Omega} = 0. \end{cases} \tag{1.5}$$

The precise statement of this result is given in the following theorem.

Theorem 1.1 *Let $\Omega \subset \mathbb{R}^2$ be a rectangle or a more general bounded and simply connected planar domain with $\partial\Omega$ belonging to $C^{2,\gamma}(\gamma \in (0,1))$ except at a finite number of points, where $\partial\Omega$ is a corner of angle in $(0, \frac{\pi}{2}]$. Assume the initial data $(\mathbf{u}_0, \theta_0) \in H^s(\Omega)$ with $s > 2$. Let $T > 0$ and assume that the solution $\mathbf{u}^{(0)}$ of (1.5) remains regular on $[0, T)$, especially*

$$\sup_{0<t<T} \|\mathbf{u}^{(0)}(t)\|_{H^s} \le M_0 < \infty. \tag{1.6}$$

Then the corresponding solution $\mathbf{u}^{(\nu)}$ of (1.4) converges to $\mathbf{u}^{(0)}$ on $[0, T)$ as $\nu \to 0$. More precisely, for any $t \le T$,

$$\begin{aligned} &\|\mathbf{u}^{(\nu)}(t) - \mathbf{u}^{(0)}(t)\|_{L^2}^2 + \|\theta^{(\nu)}(t) - \theta^{(0)}(t)\|_{L^2}^2 \\ &\quad \le C\nu t(1 + \nu + \kappa)\|\mathbf{u}^{(0)}\|_{H^2(\Omega)}^2 e^{Ct(1+\|\mathbf{u}^{(0)}\|_{H^s})}, \end{aligned} \tag{1.7}$$

where κ denotes the curvature of the boundary in the case of a general bounded domain and $\kappa = 0$ in the case of a rectangle, and C is a constant independent of ν and κ. In addition,

$$\begin{aligned} &\int_0^t \int_\Omega |\nabla(\mathbf{u}^{(\nu)} - \mathbf{u}^{(0)})(s)|^2 \, d\mathbf{x} ds + \kappa \int_0^t \int_{\partial\Omega} ((\mathbf{u}^{(\nu)} - \mathbf{u}^{(0)})(s) \cdot \tau)^2 \, d\sigma(\mathbf{x}) ds \\ &\le C t(1 + \nu + \kappa)\|\mathbf{u}^{(0)}\|_{H^2(\Omega)}^2 \Big(1 + t(1 + \|\mathbf{u}^{(0)}\|_{H^s}) e^{Ct(1+\|\mathbf{u}^{(0)}\|_{H^s})}\Big), \end{aligned} \tag{1.8}$$

where τ denotes the unit tangent vector along the boundary of $\partial\Omega$.

Theorem 1.1 states that for a general bounded domain with a smooth boundary (except for a finite number of corner points), the solution of the inviscid 2D Boussinesq system with a no-penetration boundary condition can be approximated by the corresponding solution of the Boussinesq system with velocity dissipation and a stress-free boundary condition. Moreover, this theorem establishes an explicit convergence rate of order $\sqrt{\nu t}$ at which the viscous Boussinesq solution converges to the inviscid one in the L^2-norm as the Reynolds number tends to infinity.

From a computational perspective, our result implies that the solution of the inviscid Boussinesq equation (1.5) with the slip boundary condition can be approximated via the solution of (1.4). This is particularly useful because solving inviscid problems is notoriously challenging due to the rapid growth of their Sobolev norms. Our result ensures that one can instead compute solutions of the corresponding high-Reynolds-number system, which is more tractable numerically.

1.3 Main result of linear stability of general equilibrium

Because of their geophysical applications, it is very natural to study the stability of hydrostatic equilibrium. Mathematically, hydrostatic equilibrium is a special steady-state solution of the Boussinesq equations. Doering et al. (2018) considered the following hydrostatic equilibrium solution:

$$\mathbf{u}_{\text{he}} = \mathbf{0}, \quad \theta_{\text{he}}(x_2) = \alpha x_2 + \bar{\theta}, \quad P_{\text{he}}(x_2) = \int_0^{x_2} \theta_{\text{he}}(z)\, dz. \tag{1.9}$$

In their work, (Doering et al. 2018) rigorously established the nonlinear stability and long-time behavior of perturbations near hydrostatic equilibrium. To the best of our knowledge, (Doering et al. 2018) is the first rigorous result on the stability of hydrostatic balance and our research has inspired a body of substantial subsequent research (see, e.g., Adhikari et al. (2022); Ben Said et al. (2022); Cheng et al. (2025); Dong et al. (2021); Hu et al. (2018); Ji et al. (2022); Kukavica and Wang (2020); Lai et al. (2021); Stefanov et al. (2025); Wang (2021); Wang and Yue (2020); Wu and Zhao (2023)). In particular, Wang (2021) investigates the stability of large solutions to the Boussinesq equations with Navier boundary conditions, which is related to the present work.

In the modeling of real geophysical fluids, the temperature profile is not necessarily a simple linear function of x_2 such as αx_2. Therefore, it is essential to investigate the stability of a more general hydrostatic equilibrium. In this paper, we establish a new stability result for the more general temperature profile:

$$\mathbf{u}_{\text{he}} = \mathbf{0}, \quad \theta_{\text{he}}(x_2) = H(x_2), \quad P_{\text{he}}(x_2) = \int_0^{x_2} H(z)\, dz, \tag{1.10}$$

where $H(x_2)$ is a general given function. The perturbation near the profile in (1.10), namely

$$\widetilde{\mathbf{u}} = \mathbf{u} - \mathbf{u}_{\text{he}}, \quad \widetilde{P} = P - P_{\text{he}}(x_2), \quad \widetilde{\theta} = \theta - \theta_{\text{he}}(x_2) \tag{1.11}$$

satisfies

$$\begin{cases} \partial_t \widetilde{\mathbf{u}} + \widetilde{\mathbf{u}} \cdot \nabla \widetilde{\mathbf{u}} + \nabla \widetilde{P} = \nu \Delta \widetilde{\mathbf{u}} + \widetilde{\theta} \mathbf{e}_2, \\ \partial_t \widetilde{\theta} + \widetilde{\mathbf{u}} \cdot \nabla \widetilde{\theta} + \widetilde{u}_2\, H'(x_2) = 0, \\ \nabla \cdot \widetilde{\mathbf{u}} = 0, \\ (\widetilde{\mathbf{u}}, \widetilde{\theta})(\mathbf{x}, 0) = (\widetilde{\mathbf{u}}_0, \widetilde{\theta}_0)(\mathbf{x}), \\ \widetilde{\mathbf{u}} \cdot \mathbf{n}|_{\partial\Omega} = 0, \quad \widetilde{\omega}|_{\partial\Omega} = 0, \end{cases} \tag{1.12}$$

where $\widetilde{\omega} = \nabla \times \widetilde{\mathbf{u}}$ denotes the corresponding vorticity.

The stability problem associated with (1.12) presents significant challenges. In general, nonlinear stability is not expected for an arbitrary profile, even under the condition $H'(x_2) >$

0. However, we establish a linear stability result, as stated in the following theorem. For notational convenience, we omit the tilde notation in variables representing perturbations. The corresponding linearized equations, expressed in terms of the stream function ψ and the temperature θ is given by

$$\partial_t \Delta\psi - \nu\Delta\Delta\psi - \partial_1\theta = 0, \tag{1.13}$$

$$\partial_t\theta + u_2 H'(x_2) = 0,$$

$$\psi(x_0) = \psi_0(x), \ \ \theta(x,0) = \theta_0(x). \tag{1.14}$$

Recall that the vorticity $\omega = \Delta\psi$.

Theorem 1.2 *Consider the linearied Boussinesq equations (1.13) and (1.14) near the general hydrostatic equilibrium* (1.11)*. Assume that the temperature profile $H(x_2)$ satisfies, for any point $(x_1, x_2) \in \Omega$,*

$$|H'(x_2)| \leq M.$$

Let (ψ_0, θ_0) be the initial perturbation satisfying $\partial_1\psi_0$, $\nabla\Delta\psi_0$ and θ_0 are all in $L^2(\Omega)$. Then, for $H'(x_2) > 0$, we have the following global and uniform upper bound

$$\|\partial_t\nabla\psi(t)\|^2_{L^2(\Omega)} + \int_\Omega H'(x_2)(\partial_1\psi)^2\, d\mathbf{x} + 2\nu\int_0^t \|\partial_s\Delta\psi(s)\|^2_{L^2(\Omega)} ds$$

$$\leq \nu\left(\|\nabla\Delta\psi_0\|^2_{L^2} + \|\theta_0\|^2_{L^2(\Omega)}\right) + \int_\Omega H'(x_2)(\partial_1\psi_0)^2\, d\mathbf{x}, \tag{1.15}$$

$$\|\partial_{tt}\theta(t)\|_{L^2} \leq M\sqrt{\nu\left(\|\nabla\Delta\psi_0\|^2_{L^2} + \|\theta_0\|^2_{L^2(\Omega)}\right) + \int_\Omega H'(x_2)(\partial_1\psi_0)^2\, d\mathbf{x}}. \tag{1.16}$$

We remark that direct energy estimates applied to (1.13) and (1.14) would not yield any uniform (in time) upper bound due to the presence of $H'(x_2)$ (except for the linear profile when $H'(x_2)$ is a constant). Therefore, in order to prove Theorem 1.2, we first undiscovered the wave structure hidden in (1.12) (see Lemma 3.1), which plays a crucial role in obtaining the bounds in Theorem 1.2. The last paragraph of Section 4.1.2 and Figure 4 are devoted to the numerical verification of Theorem 1.2.

The rest of this paper is divided into four sections. Section 2 proves Theorem 1.1. Section 3 presents the wave structure and the proof of Theorem 1.2. Section 4 provides important observations from numerical simulations. Section 5 gives the conclusions and discussions.

2 Inviscid limit under slip boundary condition

This section is devoted to the proof of Theorem 1.1. To serve this purpose, we first recall the following global existence and uniqueness result on (1.4). The work of Doering et al. (2018) has extensively studied the behavior of the solution of (1.1), including the following result.

Theorem 2.1 *Let $\Omega \subset \mathbb{R}^2$ be a rectangle or a more general bounded and simply connected planar domain with $\partial\Omega$ belonging to $C^{2,\gamma}(\gamma \in (0,1))$ except at a finite number of points, where $\partial\Omega$ is a corner of angle in $(0, \frac{\pi}{2}]$. Consider the initial-boundary value problem* (1.4)*. Suppose that the initial data $\mathbf{u}_0 \in H^2(\Omega)$ and $\theta_0 \in H^1(\Omega)$, $\nabla\cdot\mathbf{u}_0 = 0$ and are compatible with the boundary conditions. Then* (1.4) *has a unique global-in-time solution $(\mathbf{u}^{(\nu)}, \theta^{(\nu)})$ satisfying*

$$\mathbf{u}^{(\nu)} \in L^\infty((0,t); H^2(\Omega)) \cap L^2((0,t); H^3(\Omega)) \ \ \textit{and} \ \ \theta^{(\nu)} \in L^\infty((0,t); H^1(\Omega)) \tag{2.1}$$

for any $t > 0$*. In addition, if* $(\mathbf{u}_0, \theta_0) \in H^s(\Omega)$ *with* $s > 2$*, then* $\mathbf{u}^{(\nu)} \in L^\infty((0,t); H^s(\Omega)) \cap L^2((0,t); H^{s+1}(\Omega))$ *and* $\theta^{(\nu)} \in L^\infty((0,t); H^s(\Omega))$ *for any* $t > 0$.

The existence and regularity problem on the inviscid Boussinesq equation (1.5) is not fully understood. Whether classical solutions to (1.5) are always global in time remains an outstanding open problem. The following local existence and regularity suffices for our purpose (see, e.g., Wu (2012)).

Theorem 2.2 *Let* $\Omega \subset \mathbb{R}^2$ *be a rectangle or a more general bounded and simply connected planar domain with* $\partial\Omega$ *belonging to* $C^{2,\gamma}(\gamma \in (0,1))$ *except at a finite number of points, where* $\partial\Omega$ *is a corner of angle in* $(0, \frac{\pi}{2}]$*. Consider the initial-boundary value problem* (1.5)*. Assume that* $(\mathbf{u}_0, \theta_0) \in H^s(\Omega)$ *with* $s > 2$*. Then there is a* $T = T(\|(\mathbf{u}_0, \theta_0)\|_{H^s}) > 0$ *such that* (1.5) *has a unique solutions* $(\mathbf{u}, \theta) \in C([0,T); H^s(\Omega)$*. Furthermore, if*

$$\int_0^{T^*} \|\nabla \mathbf{u}(t)\|_{L^\infty} dt < \infty \quad \textit{or} \quad \int_0^{T^*} \|\nabla \theta(t)\|_{L^\infty} dt < \infty,$$

then the local solution can be extended to $[0, T^*]$.

In order to prove Theorem 1.1, we also need a simple fact that the slip boundary condition

$$\mathbf{u}^{(\nu)} \cdot \mathbf{n}|_{\partial\Omega} = 0, \qquad \omega^{(\nu)}|_{\partial\Omega} = 0 \tag{2.2}$$

is a special case of the Navier-slip boundary condition. Recall that the general Navier-slip boundary condition involving a velocity field $\mathbf{v}$ is given by

$$\mathbf{v} \cdot \mathbf{n} = 0, \quad \nu(S(\mathbf{v})\mathbf{n}) \cdot \tau + \alpha \mathbf{v} \cdot \tau = 0, \qquad \mathbf{x} \in \partial\Omega,$$

where $S(\mathbf{v}) = \frac{1}{2}(\nabla\mathbf{v} + (\nabla\mathbf{v}))^T)$, $\mathbf{n}(\mathbf{x})$ and $\tau(\mathbf{x})$ are the outward unit normal and a unit tangent to $\partial\Omega$, and $\alpha(\mathbf{x})$ is a non-negative turbulent boundary drag coefficient defined on $\partial\Omega$.

The stress-free boundary condition (2.2) can be viewed as a special Navier-slip boundary condition, as the following lemma states (see, e.g., Doering et al. (2018); Jiu et al. (2012)).

Lemma 2.3 *For any* $\mathbf{v} \in H^2(\Omega)$ *with* $\mathbf{v} \cdot \mathbf{n} = 0$ *on* $\partial\Omega$*, we have*

$$(S(\mathbf{v})\mathbf{n}) \cdot \tau + \kappa \mathbf{v} \cdot \tau = \frac{1}{2}\omega, \qquad \mathbf{x} \in \partial\Omega,$$

where κ *is the curvature of* $\partial\Omega$ *and* $\omega = \nabla \times \mathbf{v}$ *is the vorticity. In particular, if* $\omega = 0$ *on* $\partial\Omega$*, then the following Navier-slip boundary condition holds*

$$(S(\mathbf{v})\mathbf{n}) \cdot \tau + \kappa \mathbf{v} \cdot \tau = 0.$$

We are now ready to prove Theorem 1.1.

Proof of Theorem 1.1 We set

$$\mathbf{V} = \mathbf{u}^{(\nu)} - \mathbf{u}^{(0)}, \quad \Theta = \theta^{(\nu)} - \theta^{(0)}.$$

Writing $\mathbf{u}^{(\nu)} = \mathbf{V} + \mathbf{u}^{(0)}$ and $\theta^{(\nu)} = \Theta + \theta^{(0)}$ in (1.4) and taking the difference with (1.5), we find that

$$\begin{cases} \partial_t \mathbf{V} + \mathbf{V} \cdot \nabla \mathbf{u}^{(0)} + \mathbf{u}^{(0)} \cdot \nabla \mathbf{V} + \mathbf{V} \cdot \nabla \mathbf{V} = -\nabla P + \nu \Delta \mathbf{u}^{(\nu)} \Theta \mathbf{e}_2, \quad x \in \Omega, t > 0, \\ \partial_t \Theta + \Theta \cdot \nabla \theta^{(0)} + \mathbf{u}^{(0)} \cdot \nabla \Theta + \mathbf{V} \cdot \nabla \Theta = 0, \\ \nabla \cdot \mathbf{V} = 0, \\ \mathbf{V} \cdot \mathbf{n}|_{\partial\Omega} = 0, \end{cases} \tag{2.3}$$

where $P = p^{(\nu)} - p^{(0)}$ is the pressure difference. Taking the inner product of $\mathbf{V}$ and Θ with the first two equations of (2.3), we find that

$$\frac{1}{2}\frac{d}{dt}\left(\|\mathbf{V}\|_{L^2}^2 + \|\Theta\|_{L^2}^2\right) \tag{2.4}$$

$$= -\int_\Omega \mathbf{V}\cdot\nabla\mathbf{u}^{(0)}\cdot\mathbf{V}\,d\mathbf{x} - \int_\Omega \Theta\cdot\nabla\mathbf{u}^{(0)}\cdot\Theta\,d\mathbf{x} + \nu\int_\Omega \mathbf{V}\cdot\Delta\mathbf{u}^{(0)}\,d\mathbf{x} + \nu\int_\Omega \mathbf{V}\cdot\Delta\mathbf{V}\,d\mathbf{x}$$

$$:= I_1 + I_2 + I_3 + I_4. \tag{2.5}$$

where we have applied the boundary conditions $\mathbf{V}\cdot\mathbf{n}|_{\partial\Omega} = \mathbf{u}^{(0)}\cdot\mathbf{n}|_{\partial\Omega} = 0$ and the Divergence Theorem to obtain

$$\int_\Omega (\mathbf{u}^{(0)}\cdot\nabla)\mathbf{V}\cdot\mathbf{V}\,d\mathbf{x} = \int_\Omega (\mathbf{V}\cdot\nabla)\mathbf{V}\cdot\mathbf{V}\,d\mathbf{x} = \int_\Omega \Theta(\mathbf{u}^{(0)}\cdot\nabla)\Theta\,d\mathbf{x} = \int_\Omega \Theta(\mathbf{V}\cdot\nabla)\Theta\,d\mathbf{x} = 0.$$

I_1 and I_2 can be bounded directly via (1.6). By Sobolev's inequality,

$$|I_1 + I_2| \le \|\nabla\mathbf{u}^{(0)}\|_{L^\infty(\Omega)}\left(\|\mathbf{V}\|_{L^2}^2 + \|\Theta\|_{L^2}^2\right) \le C\,\|\mathbf{u}^{(0)}\|_{H^s}\left(\|\mathbf{V}\|_{L^2}^2 + \|\Theta\|_{L^2}^2\right). \tag{2.6}$$

By Hölder's inequality,

$$|I_3| \le \nu\|\mathbf{V}\|_{L^2}\,\|\Delta\mathbf{u}^{(0)}\|_{L^2} \le \frac{1}{4}\|\mathbf{V}\|_{L^2}^2 + \nu^2\|\Delta\mathbf{u}^{(0)}\|_{L^2}^2. \tag{2.7}$$

The estimate of I_4 is more delicate. We distinguish two cases: a general bounded domain and the rectangle. When Ω is a general bounded domain, we use Lemma 2.3 and the boundary condition $\omega^{(\nu)}|_{\partial\Omega} = 0$ for the vorticity $\omega^{(\nu)}$ of (1.4). Due to $\nabla\cdot\mathbf{V} = 0$,

$$\begin{aligned}
\mathbf{V}\cdot\Delta\mathbf{V} &= \sum_{j,k=1}^{2}\mathbf{V}_j\partial_k^2 V_j = \sum_{j,k=1}^{2}\mathbf{V}_j\partial_k(\partial_k\mathbf{V}_j + \partial_j\mathbf{V}_k)\\
&= \sum_{j,k=1}^{2}\partial_k(\mathbf{V}_j(\partial_k\mathbf{V}_j + \partial_j\mathbf{V}_k)) - \sum_{j,k=1}^{2}(\partial_k\mathbf{V}_j)^2 - \sum_{j,k=1}^{2}\partial_k\mathbf{V}_j\partial_j\mathbf{V}_k\\
&= 2\sum_{j,k=1}^{2}\partial_k(\mathbf{V}_j S(\mathbf{V})_{kj}) - |\nabla\mathbf{V}|^2 - \sum_{j,k=1}^{2}\partial_k\mathbf{V}_j\partial_j\mathbf{V}_k,
\end{aligned}$$

where we have recalled that $S(\mathbf{V})$ denotes the symmetric part of $\nabla\mathbf{V}$, namely

$$S(\mathbf{V}) = \frac{1}{2}(\nabla\mathbf{V} + (\nabla\mathbf{V})^T).$$

Therefore, by the divergence theorem,

$$\begin{aligned}
I_4 := \nu\int_\Omega \mathbf{V}\cdot\Delta\mathbf{V}\,d\mathbf{x} &= 2\nu\int_\Omega \nabla\cdot(\mathbf{V}S(\mathbf{V}))\,d\mathbf{x} - \nu\int_\Omega |\nabla\mathbf{V}|^2\,d\mathbf{x}\\
&\quad - \nu\sum_{j,k=1}^{2}\int_\Omega \partial_k\mathbf{V}_j\partial_j\mathbf{V}_k\,d\mathbf{x}\\
&= 2\nu\int_{\partial\Omega}\mathbf{V}\cdot(S(\mathbf{V})\mathbf{n})\,d\sigma(\mathbf{x}) - \nu\int_\Omega |\nabla\mathbf{V}|^2\,d\mathbf{x},
\end{aligned} \tag{2.8}$$

where the last integral becomes zero after integration by parts and the use of $\nabla \cdot \mathbf{V} = 0$. We decompose $\mathbf{V}$ and $S(\mathbf{V})\mathbf{n}$ each in th directions of $\mathbf{n}$ and τ. Due to $\mathbf{V} \cdot \mathbf{n} = 0$ on $\partial\Omega$,

$$\begin{aligned} \mathbf{V} &= (\mathbf{V} \cdot \mathbf{n})\mathbf{n} + (\mathbf{V} \cdot \tau)\tau = (\mathbf{V} \cdot \tau)\tau, \\ S(\mathbf{V})\mathbf{n} &= ((S(\mathbf{V})\mathbf{n}) \cdot \mathbf{n})\mathbf{n} + ((S(\mathbf{V})\mathbf{n}) \cdot \tau)\tau. \end{aligned}$$

Since $\mathbf{n}$ and τ are orthogonal, namely $\mathbf{n} \cdot \tau = 0$,

$$\mathbf{V} \cdot (S(\mathbf{V})\mathbf{n}) = (\mathbf{V} \cdot \tau)\,((S(\mathbf{V})\mathbf{n}) \cdot \tau).$$

To use the boundary condition $\omega^{(\nu)}|_{\partial\Omega} = 0$, we recall $\mathbf{V} = \mathbf{u}^{(\nu)} - \mathbf{u}^{(0)}$ and use Lemma 2.3 to obtain

$$\begin{aligned} (S(\mathbf{V})\mathbf{n}) \cdot \tau &= (S(\mathbf{u}^{(\nu)})\mathbf{n}) \cdot \tau - (S(\mathbf{u}^{(0)})\mathbf{n}) \cdot \tau \\ &= -\kappa \mathbf{u}^{(\nu)} \cdot \tau - (S(\mathbf{u}^{(0)})\mathbf{n}) \cdot \tau \\ &= -\kappa \mathbf{V} \cdot \tau - \kappa \mathbf{u}^{(0)} \cdot \tau - (S(\mathbf{u}^{(0)})\mathbf{n}) \cdot \tau. \end{aligned}$$

Therefore,

$$\mathbf{V} \cdot (S(\mathbf{V})\mathbf{n}) = -\kappa (\mathbf{V} \cdot \tau)^2 - \kappa (\mathbf{V} \cdot \tau)(\mathbf{u}^{(0)} \cdot \tau) - (\mathbf{V} \cdot \tau)(S(\mathbf{u}^{(0)})\mathbf{n}) \cdot \tau. \tag{2.9}$$

Inserting (2.9) in (2.8), we obtain

$$\begin{aligned} \nu \int_\Omega \mathbf{V} \cdot \Delta \mathbf{V}\, d\mathbf{x} = &-2\nu\kappa \int_{\partial\Omega} (\mathbf{V} \cdot \tau)^2\, d\sigma(\mathbf{x}) - \nu \int_\Omega |\nabla \mathbf{V}|^2\, d\mathbf{x} \\ &- 2\nu\kappa \int_{\partial\Omega} (\mathbf{V} \cdot \tau)(\mathbf{u}^{(0)} \cdot \tau)\, d\sigma(\mathbf{x}) \\ &- 2\nu \int_{\partial\Omega} (\mathbf{V} \cdot \tau)(S(\mathbf{u}^{(0)})\mathbf{n}) \cdot \tau\, d\sigma(\mathbf{x}). \end{aligned} \tag{2.10}$$

The last two terms in (2.10) can be bounded as follows. By the trace theorem, the L^2-norm of $\mathbf{u}^{(0)}$ on $\partial\Omega$ is bounded by the H^1-norm of $\mathbf{u}^{(0)}$ on Ω,

$$\begin{aligned} 2\nu\kappa \int_{\partial\Omega} (\mathbf{V} \cdot \tau)(\mathbf{u}^{(0)} \cdot \tau)\, d\sigma(\mathbf{x}) &\le \nu\kappa \int_{\partial\Omega} (\mathbf{V} \cdot \tau)^2\, d\sigma(\mathbf{x}) + \nu\kappa \int_{\partial\Omega} (\mathbf{u}^{(0)} \cdot \tau)^2\, d\sigma(\mathbf{x}) \\ &\le \nu\kappa \int_{\partial\Omega} (\mathbf{V} \cdot \tau)^2\, d\sigma(\mathbf{x}) + C\, \nu\kappa \|\mathbf{u}^{(0)}\|_{H^1(\Omega)}^2, \end{aligned} \tag{2.11}$$

where C is a constant independent of ν. By Hölder's inequality, $|\mathbf{V} \cdot \tau| \le |\mathbf{V}|$ and the trace theorem,

$$\begin{aligned} &2\nu \int_{\partial\Omega} (\mathbf{V} \cdot \tau)(S(\mathbf{u}^{(0)})\mathbf{n}) \cdot \tau\, d\sigma(\mathbf{x}) \\ &\le 2\nu \|\mathbf{V}\|_{L^2(\partial\Omega)} \|S(\mathbf{u}^{(0)})\|_{L^2(\partial\Omega)} \\ &\le C\, \nu \|\mathbf{V}\|_{H^1(\Omega)}\, \|S(\mathbf{u}^{(0)})\|_{H^1(\Omega)} \\ &\le C\, \nu (\|\mathbf{V}\|_{L^2(\Omega)} + \|\nabla \mathbf{V}\|_{L^2(\Omega)})\, \|\nabla \mathbf{u}^{(0)}\|_{H^1(\Omega)} \\ &\le C \|\mathbf{V}\|_{L^2(\Omega)}^2 + \nu^2 \|\mathbf{u}^{(0)}\|_{H^2(\Omega)}^2 + \frac{1}{2}\nu \|\nabla \mathbf{V}\|_{L^2(\Omega)}^2 + C\nu\, \|\mathbf{u}^{(0)}\|_{H^2(\Omega)}^2. \end{aligned} \tag{2.12}$$

Inserting (2.11) and (2.12) in (2.10) yields

$$I_4 := \nu \int_\Omega \mathbf{V} \cdot \Delta \mathbf{V}\, d\mathbf{x} \le -\nu\kappa \int_{\partial\Omega} (\mathbf{V}\cdot\tau)^2\, d\sigma(\mathbf{x}) - \frac{1}{2}\nu \int_\Omega |\nabla \mathbf{V}|^2\, d\mathbf{x} + C\|\mathbf{V}\|^2_{L^2(\Omega)} + C(\nu + \nu\kappa + \nu^2)\, \|\mathbf{u}^{(0)}\|^2_{H^2(\Omega)}. \tag{2.13}$$

Combining (2.5) with the bounds in (2.6), (2.7) and (2.13), we obtain

$$\frac{1}{2}\frac{d}{dt}\left(\|\mathbf{V}\|^2_{L^2} + \|\Theta\|^2_{L^2}\right) + \frac{1}{2}\nu \int_\Omega |\nabla \mathbf{V}|^2\, d\mathbf{x} + \nu\kappa \int_{\partial\Omega} (\mathbf{V}\cdot\tau)^2\, d\sigma(\mathbf{x}) \le C\,(1 + \|\mathbf{u}^{(0)}\|_{H^s})\left(\|\mathbf{V}\|^2_{L^2} + \|\Theta\|^2_{L^2}\right) + C(\nu + \nu\kappa + \nu^2)\, \|\mathbf{u}^{(0)}\|^2_{H^2(\Omega)}. \tag{2.14}$$

Applying Gronwall's inequality to (2.14), we obtain

$$\begin{aligned}
&\|\mathbf{V}(t)\|^2_{L^2} + \|\Theta(t)\|^2_{L^2} \\
&\quad\le e^{C\,t(1+\|\mathbf{u}^{(0)}\|_{H^s})}\left[\left(\|\mathbf{V}(0)\|^2_{L^2} + \|\Theta(0)\|^2_{L^2}\right) + C\nu t(1+\nu+\kappa)\|\mathbf{u}^{(0)}\|^2_{H^2(\Omega)}\right] \\
&\quad\le C\,\nu t(1+\nu+\kappa)\|\mathbf{u}^{(0)}\|^2_{H^2(\Omega)} e^{C\,t(1+\|\mathbf{u}^{(0)}\|_{H^s})},
\end{aligned} \tag{2.15}$$

where we have used the fact that the initial difference $(\mathbf{V}(0), \Theta(0)) = 0$. In addition, inserting (2.15) on the right-hand side of (2.14) and integrating it time, we have

$$\nu \int_0^t \int_\Omega |\nabla \mathbf{V}|^2\, d\mathbf{x} d\tau + \nu\kappa \int_0^t \int_{\partial\Omega} (\mathbf{V}\cdot\tau)^2\, d\sigma(\mathbf{x}) d\tau \le C\,\nu t(1+\nu+\kappa)\|\mathbf{u}^{(0)}\|^2_{H^2(\Omega)}\left(1 + t(1+\|\mathbf{u}^{(0)}\|_{H^s}) e^{C\,t(1+\|\mathbf{u}^{(0)}\|_{H^s})}\right). \tag{2.16}$$

This finishes the proof of (1.7).

In the case when Ω is just a rectangle, the upper bounds for I_1, I_2 and I_3 remain the same. But the estimate for the dissipative term is different. We integrate by part directly, recalling that $\mathbf{V} = u^{(\nu)} - u^{(0)}$

$$I_4 := \nu \int_\Omega \mathbf{V} \cdot \Delta \mathbf{V}\, d\mathbf{x} = \sum_{j,k=1}^{2} \nu \int_\Omega \mathbf{V}_j \partial_k^2 \mathbf{u}_j^{(\nu)}\, d\mathbf{x} - \sum_{j,k=1}^{2} \nu \int_\Omega \mathbf{V}_j \partial_k^2 \mathbf{u}_j^{(0)}\, d\mathbf{x} := I_{41} + I_{42}.$$

By the divergence theorem,

$$I_{41} = \sum_{j,k=1}^{2} \nu \int_\Omega \mathbf{V}_j \partial_k^2 \mathbf{u}_j^{(\nu)}\, d\mathbf{x} = \sum_{j,k=1}^{2} \nu \int_{\partial\Omega} \mathbf{V}_j \mathbf{n}_k \partial_k \mathbf{u}_j^{(\nu)}\, d\sigma(\mathbf{x}) - \sum_{j,k=1}^{2} \nu \int_\Omega \partial_k \mathbf{V}_j \partial_k \mathbf{u}_j^{(\nu)}\, d\mathbf{x}$$

When Ω is a rectangle, $\partial\Omega$ consists of four line segments. Using the boundary conditions

$$\mathbf{V}\cdot\mathbf{n} = 0, \quad \omega^{(\nu)} = 0,$$

we can show that the boundary term

$$\int_{\partial\Omega} \mathbf{V}_j \mathbf{n}_k \partial_k \mathbf{u}_j^{(\nu)}\, d\sigma(\mathbf{x}) = 0.$$

For example, on the line segment $\partial\Omega_1$ with $0 \le x_1 \le 1$ and $x_2 = 0$, we have

$$\mathbf{V} = (V_1, 0), \quad \mathbf{n} = (0, -1), \quad \omega^{(\nu)} = \partial_1 u_2^{(\nu)} - \partial_2 u_1^{(\nu)} = -\partial_2 u_1^{(\nu)} = 0$$

and thus

$$\sum_{j,k=1}^{2} \nu \int_{\partial\Omega_1} \mathbf{V}_j \mathbf{n}_k \partial_k \mathbf{u}_j^{(\nu)}\, d\sigma(\mathbf{x}) = -\nu \int_{\partial\Omega_1} V_1 \partial_2 u_1^{(\nu)} d\sigma(\mathbf{x}) = 0.$$

Similarly, the boundary integral on the other three lines are also zero. Therefore,

$$\begin{aligned} I_{41} &= -\sum_{j,k=1}^{2} \nu \int_\Omega \partial_k \mathbf{V}_j \partial_k \mathbf{u}_j^{(\nu)}\, d\mathbf{x} \\ &= -\sum_{j,k=1}^{2} \nu \int_\Omega \partial_k \mathbf{V}_j \partial_k \mathbf{V}_j\, d\mathbf{x} + \sum_{j,k=1}^{2} \nu \int_\Omega \partial_k \mathbf{V}_j \partial_k \mathbf{u}_j^{(0)}\, d\mathbf{x} \\ &= -\nu \|\nabla \mathbf{V}\|_{L^2}^2 + \nu \int_\Omega \nabla \mathbf{V} \cdot \nabla \mathbf{u}^{(0)}\, d\mathbf{x} \\ &\le -\frac{1}{2}\nu \|\nabla \mathbf{V}\|_{L^2}^2 + \nu \|\nabla \mathbf{u}^{(0)}\|_{L^2}^2. \end{aligned} \tag{2.17}$$

By Hölder's inequality,

$$|I_{42}| \le \nu \|\mathbf{V}\|_{L^2} \|\Delta \mathbf{u}^{(0)}\|_{L^2} \le \frac{1}{4}\|\mathbf{V}\|_{L^2} + \nu^2 \|\Delta \mathbf{u}^{(0)}\|_{L^2}^2. \tag{2.18}$$

After inserting (2.6), (2.7), (2.17) and (2.18) in (2.5), we have

$$\begin{aligned} &\frac{1}{2}\frac{d}{dt}\left(\|\mathbf{V}\|_{L^2}^2 + \|\Theta\|_{L^2}^2\right) + \frac{1}{2}\nu \int_\Omega |\nabla \mathbf{V}|^2\, d\mathbf{x} \\ &\quad \le C\,(1 + \|\mathbf{u}^{(0)}\|_{H^s})\left(\|\mathbf{V}\|_{L^2}^2 + \|\Theta\|_{L^2}^2\right) + C\nu(1+\nu)\,\|\mathbf{u}^{(0)}\|_{H^2(\Omega)}^2. \end{aligned} \tag{2.19}$$

It then follows from Gronwall's inequality that

$$\|\mathbf{V}(t)\|_{L^2}^2 + \|\Theta(t)\|_{L^2}^2 \le C\,\nu t(1+\nu)\,\|\mathbf{u}^{(0)}\|_{H^2(\Omega)}^2 e^{C\,t(1+\|\mathbf{u}^{(0)}\|_{H^s})}. \tag{2.20}$$

Applying the bound in (2.20) to the right of (2.19) and integrating in time, we obtain the time integral bound

$$\nu \int_0^t |\nabla \mathbf{V}|^2\, d\mathbf{x}\, d\tau \le C\,\nu t(1+\nu)\|\mathbf{u}^{(0)}\|_{H^2(\Omega)}^2 \Big(1 + t(1 + \|\mathbf{u}^{(0)}\|_{H^s}) e^{C\,t(1+\|\mathbf{u}^{(0)}\|_{H^s})}\Big).$$

This completes the proof of Theorem 1.1. □

3 Linear stability of a general hydrostatic equilibrium

This section proves the linear stability result of a general hydrostatic equilibrium profile (1.10), namely Theorem 1.2.

To avoid the pressure term, we take advantage of the equivalent vorticity formulation of (1.12),

$$\begin{cases} \partial_t \widetilde{\omega} + \widetilde{\mathbf{u}} \cdot \nabla \widetilde{\omega} = \nu \Delta \widetilde{\omega} + \partial_{x_1} \widetilde{\theta}, \\ \partial_t \widetilde{\theta} + \widetilde{\mathbf{u}} \cdot \nabla \widetilde{\theta} + \widetilde{u}_2\, H'(x_2) = 0, \\ \nabla \cdot \widetilde{\mathbf{u}} = 0, \\ \widetilde{\mathbf{u}} \cdot \mathbf{n}|_{\partial\Omega} = 0, \quad \widetilde{\omega}|_{\partial\Omega} = 0, \end{cases} \tag{3.1}$$

We discover that (3.1) actually has a hidden wave structure, as revealed in the following lemma. For notational convenience, we will ignore tilde and write f for $\widetilde{f}$.

Lemma 3.1 *If (ω, θ) solves (3.1), then $\mathbf{u}$, ω and θ satisfies the following wave equations*

$$\partial_{tt}\omega - \nu\Delta\partial_t\omega + H'(x_2)\,\partial_{11}\Delta^{-1}\omega = N_3, \tag{3.2}$$

$$\partial_{tt}\mathbf{u} - \nu\Delta\partial_t\mathbf{u} + H'(x_2)\,\partial_{11}\Delta^{-1}\mathbf{u} = N_4, \tag{3.3}$$

$$\partial_{tt}\theta - \nu\Delta\partial_t\theta + H'(x_2)\,\partial_{11}\Delta^{-1}\theta = 2H''(x_2)\partial_1\partial_2\psi - H'''(x_2)\partial_1\psi + N_5, \tag{3.4}$$

where N_3, N_4 and N_5 are nonlinear terms

$$N_3 = \partial_1 N_2 - \partial_t N_1, \quad N_4 = \nabla^{\perp}\Delta^{-1}(\partial_1 N_2 - \partial_t N_1),$$
$$N_5 = H'(x_2)\partial_1\Delta^{-1}N_1 - (\partial_t - \nu\Delta)N_2$$

with $N_1 = \mathbf{u}\cdot\nabla\omega$ and $N_2 = \mathbf{u}\cdot\nabla\theta$. As a special consequence, when $H'(x_2) = A$ for a constant A, then the linearized equation for ω, $\mathbf{u}$ and θ is identically the same and given by

$$\partial_{tt}\Phi - \nu\Delta\partial_t\Phi + A\,\partial_{11}\Delta^{-1}\Phi = 0.$$

The wave structure derived in Lemma 3.1 reveals the hidden interaction between fluid velocity, vorticity, and temperature near hydrostatic balance. The additional linear terms $H'(x_2)\partial_{11}\Delta^{-1}\mathbf{u}$ and $H'(x_2)\partial_{11}\Delta^{-1}\omega$, which are not initially present in the velocity and vorticity equations, emerge as a consequence of hydrostatic equilibrium and interaction. When $H(x_2)$ is not a linear function, the wave equation for θ is different from those for velocity and vorticity and contains two extra linear terms besides the nonlinear terms.

Proof of Lemma 3.1 Since $\nabla\cdot\mathbf{u} = 0$, we write $\mathbf{u}$ in terms of the stream function ψ,

$$\mathbf{u} = \nabla^{\perp}\psi = (-\partial_2\psi, \partial_1\psi)$$

and then $\omega = \Delta\psi$. Then (3.1) can be written as

$$\begin{cases} \partial_t\Delta\psi - \nu\Delta\Delta\psi - \partial_1\theta = -N_1, & N_1 = \mathbf{u}\cdot\nabla\Delta\psi, \\ \partial_t\theta + \partial_1\psi H'(x_2) = -N_2, & N_2 = \mathbf{u}\cdot\nabla\theta. \end{cases} \tag{3.5}$$

Taking the time derivative of the first equation of (3.5) yields

$$\partial_{tt}\Delta\psi - \nu\Delta\partial_t(\Delta\psi) - \partial_1\partial_t\theta = -\partial_t N_1. \tag{3.6}$$

Inserting the equation of θ in (3.6), we find

$$\partial_{tt}\Delta\psi - \nu\Delta\partial_t(\Delta\psi) - \partial_1(-\partial_1\psi H'(x_2)) = \partial_1 N_2 - \partial_t N_1$$

or

$$\partial_{tt}\Delta\psi - \nu\Delta\partial_t(\Delta\psi) + H'(x_2)\,\partial_{11}\psi = \partial_1 N_2 - \partial_t N_1, \tag{3.7}$$

which is the desired wave equation of ψ. Without loss of generality, we take $\psi = 0$ on the boundary $\partial\Omega$ and we can then invert the equation

$$\Delta\psi = \omega$$

to write $\psi = \Delta^{-1}\omega$. Then (3.7) can be rewritten as

$$\partial_{tt}\omega - \nu\Delta\partial_t\omega + H'(x_2)\,\partial_{11}\Delta^{-1}\omega = N_3,$$

where N_3 represents the nonlinear term

$$N_3 = \partial_1 N_2 - \partial_t N_1.$$

(3.7) also allows us to write the wave equation for the velocity field $\mathbf{u}$,

$$\partial_{tt}\mathbf{u} - \nu\Delta\partial_t\mathbf{u} + H'(x_2)\,\partial_{11}\Delta^{-1}\mathbf{u} = N_4,$$

where N_4 is the corresponding nonlinear term

$$N_4 = \nabla^{\perp}\Delta^{-1}(\partial_1 N_2 - \partial_t N_1).$$

Taking ∂_t on the equation of θ in (3.5) yields

$$\partial_{tt}\theta + H'(x_2)\partial_1\partial_t\psi = -\partial_t N_2.$$

Invoking the equation of ψ, namely

$$\partial_t\psi - \nu\Delta\psi - \partial_1\Delta^{-1}\theta = -\Delta^{-1}N_1,$$

we have

$$\partial_{tt}\theta + H'(x_2)\partial_1\left(\nu\Delta\psi + \partial_1\Delta^{-1}\theta - \Delta^{-1}N_1\right) = -\partial_t N_2$$

or

$$\partial_{tt}\theta + H'(x_2)\,\partial_{11}\Delta^{-1}\theta + \nu H'(x_2)\Delta\partial_1\psi = H'(x_2)\partial_1\Delta^{-1}N_1 - \partial_t N_2.$$

By writing

$$H'(x_2)\Delta\partial_1\psi = \Delta(H'(x_2)\partial_1\psi) - 2H''(x_2)\partial_1\partial_2\psi - H'''(x_2)\partial_1\psi,$$

we obtain

$$\begin{aligned}&\partial_{tt}\theta + H'(x_2)\,\partial_{11}\Delta^{-1}\theta + \nu\Delta(H'(x_2)\partial_1\psi)\\ &\quad = 2H''(x_2)\partial_1\partial_2\psi - H'''(x_2)\partial_1\psi + H'(x_2)\partial_1\Delta^{-1}N_1 - \partial_t N_2.\end{aligned}$$

Using the equation of θ again, we have

$$\begin{aligned}&\partial_{tt}\theta + H'(x_2)\,\partial_{11}\Delta^{-1}\theta + \nu\Delta(-\partial_t\theta - N_2)\\ &\quad = 2H''(x_2)\partial_1\partial_2\psi - H'''(x_2)\partial_1\psi + H'(x_2)\partial_1\Delta^{-1}N_1 - \partial_t N_2,\end{aligned}$$

which is the desired wave equation (3.4) for θ. This completes the proof of Lemma 3.1. □

The wave structure derived in Lemma 3.1 allows to obtain a linear stability result. According to Lemma 3.1, (1.13) and (1.14) can be converted to the following wave equations

$$\begin{aligned}&\partial_{tt}\Delta\psi - \nu\Delta\partial_t\Delta\psi + H'(x_2)\,\partial_{11}\psi = 0, &(3.8)\\ &\partial_{tt}\theta - \nu\Delta\partial_t\theta + H'(x_2)\,\partial_{11}\Delta^{-1}\theta = 2H''(x_2)\partial_1\partial_2\psi - H'''(x_2)\partial_1\psi,\\ &\psi(x,0) = \psi_0(x), \quad \partial_t\psi(x,0) = \nu\Delta\psi_0 + \partial_1\Delta^{-1}\theta_0,\\ &\theta(x,0) = \theta_0(x), \quad \partial_t\theta(x,0) = \partial_1\psi_0(x)H'(x_2). &(3.9)\end{aligned}$$

We are now ready to prove Theorem 1.2.

Proof of Theorem 1.2 Multiplying (3.8) by $\partial_t\psi$ and using the factor that $\psi = 0$, $\partial_t\psi = 0$ and $\partial_t\Delta\psi = 0$ on $\partial\Omega$, we find that

$$\frac{1}{2}\frac{d}{dt}\left(\|\partial_t\nabla\psi\|^2_{L^2(\Omega)} + \int_\Omega H'(x_2)(\partial_1\psi)^2\,d\mathbf{x}\right) + \nu\|\partial_t\Delta\psi\|^2_{L^2(\Omega)} = 0.$$

Integrating in time yields

$$\begin{aligned}\|\partial_t\nabla\psi(t)\|^2_{L^2(\Omega)} &+ \int_\Omega H'(x_2)(\partial_1\psi)^2\,d\mathbf{x} + 2\nu\int_0^t \|\partial_s\Delta\psi(s)\|^2_{L^2(\Omega)}ds\\ &= \|\nabla(\nu\Delta\psi_0 + \partial_1\Delta^{-1}\theta_0)\|^2_{L^2(\Omega)} + \int_\Omega H'(x_2)(\partial_1\psi_0)^2\,d\mathbf{x},\end{aligned}$$

which yields (1.15). Due to the lack of boundary condition on θ, it does not appear possible to engage the wave equation of θ, (3.9) to gain any uniform upper bound. We use (1.14) to obtain (1.16). Applying ∂_t to (1.14) to obtain

$$\partial_{tt}\theta = -\partial_t u_2 H'(x_2).$$

Taking the L^2-norm each side yields

$$\begin{aligned}\|\partial_{tt}\theta(t)\|_{L^2} &\le M\,\|\partial_t u_2\|_{L^2} \le M\,\|\partial_t\nabla\psi\|_{L^2}\\ &\le M\sqrt{\nu\left(\|\nabla\Delta\psi_0\|^2_{L^2} + \|\theta_0\|^2_{L^2(\Omega)}\right) + \int_\Omega H'(x_2)(\partial_1\psi_0)^2\,d\mathbf{x}}.\end{aligned}$$

This completes the proof of Theorem 1.2. □

4 Numerical results

This paper conducts a detailed numerical study to understand how the sizes of the Reynolds number and the aforementioned two types of boundary conditions affect the stratification process. A range of initial data is tested. For the clarity of our presentation, we focus on the following initial condition in the domain $\Omega = (-1, 1)^2$:

$$\begin{aligned}u_{10}(x_1, x_2) &= \sin(2\pi x_1)\cos(2\pi x_2),\\ u_{20}(x_1, x_2) &= -\cos(2\pi x_1)\sin(2\pi x_2),\\ \theta_0(x_1, x_2) &= \sin(3x_1)\cos(2x_2) + (x_1 - 0.5)^3 + 1/(x_2 + 10).\end{aligned}$$

The initial temperature profile and its stratification state are plotted in Figure 1. Solutions of (1.1), supplemented with this initial data and the two boundary conditions, are computed for Reynolds numbers ranging from 0.01 to 100. The results are plotted and compared with the eventual temperature profile defined by $S(x_2)$. Here, the Reynolds number is defined as $Re = \frac{LU}{\nu}$, where $L = 2$ represents the domain size, and $U = 1$ is the characteristic velocity magnitude.

All numerical simulations are conducted using an iterative projection method outlined in Doering et al. (2018). This study explores both slip and no-slip boundary conditions, with Reynolds numbers ranging from 0.01 to 100. For each simulation, the accuracy of the results is verified by employing two levels of mesh refinement, with grid resolutions of $N = 50$ and $N = 100$, where N denotes the number of grid divisions along each spatial direction. Unlike the long-time simulations extending to $t = 10^5$ in Doering et al. (2018), the present

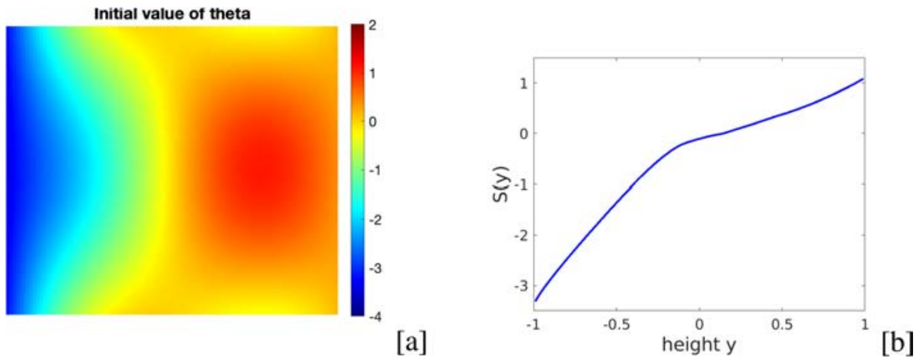

Fig. 1 **a** the initial temperature field θ_0. **b** the stratification state $S(y)$ of θ_0

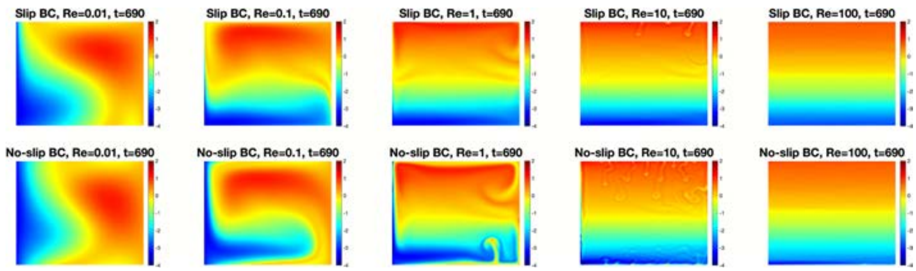

Fig. 2 Temperature fields at t=690. First row: slip boundary condition. Second row: no-slip boundary condition. Columns from left to right: $Re = 0.01, 0.1, 1, 10, 100$

study considers simulations up to $t = 690$, which is sufficient to capture the key differences arising from varying parameters and boundary conditions

4.1 Effects of Reynolds number and boundary conditions

4.1.1 Boundary persistence and plume eruption under no-slip BC

The temperature fields at $t = 690$ are plotted in Fig. 2 for both the slip and no-slip boundary conditions and all the Reynolds numbers in this study. For both types of boundaries, the stratification effect increases with the Reynolds number: the temperature field remains nearly unchanged from the initial state when $Re = 0.01$, but presents a clear stratified structure at $Re = 100$.

In particular, the simulations show two remarkable mechanisms under the no-slip boundary condition in comparison with the slip boundary condition. The first is the boundary persistence of the temperature over time under the no-slip boundary condition, which can be clearly seen on the left edge in Fig. 2 where the blue color stays the same from the initial stage when $Re = 0.1, 1, 10$, in contrast to their counterparts with the slip boundary condition. This is because the velocity is zero on the boundary under the no-slip condition, which prevents the flow along the boundary. Clearly, the boundary persistence stalls the stratification locally. The second mechanism is the boundary plume eruption, where the plumes/mushrooms are generated near the boundary and sent to the interior. There are far more boundary plume eruptions under the no-slip condition than the slip condition, especially when $Re = 10$ in

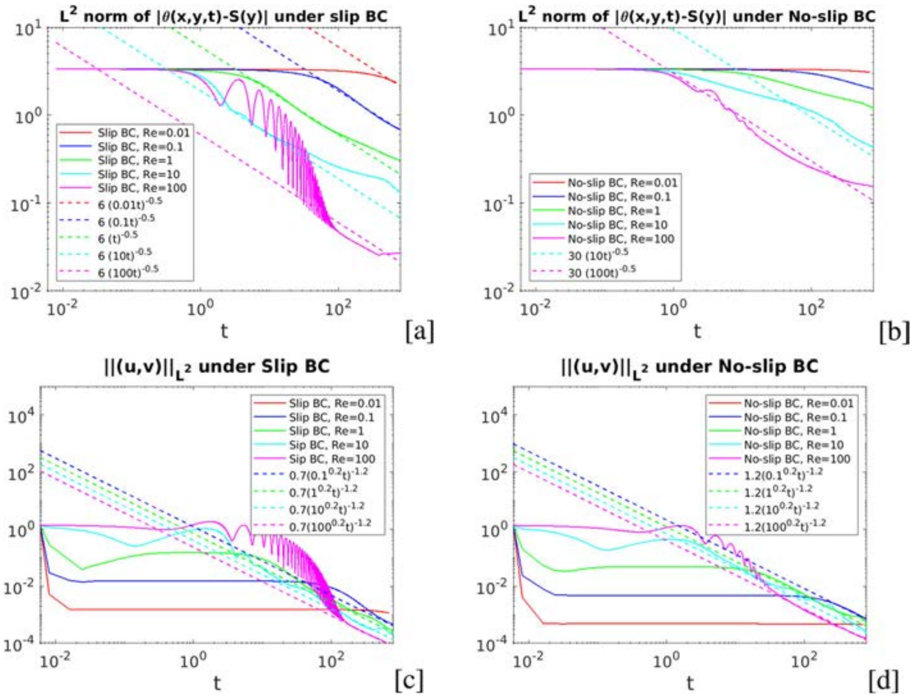

Fig. 3 **ab** $\|\theta(x,y,t) - S(y)\|_{L^2(\Omega)}$ under slip boundary condition **a** and no-slip boundary condition **b**. **cd** $\|(u,v)\|_{L^2(\Omega)}$ under slip boundary condition **c** and no-slip boundary condition **d**

Figure 2. Note the plumes near the bottom bring the high temperature upward and those near the top take the low temperature download, which promotes the stratification. Therefore, the boundary plume eruption counteracts the boundary persistence in stratification.

4.1.2 Evolution: viscous dissipation and stratification stages

We name $\|\theta(x,y,t) - S(y)\|_{L^2(\Omega)}$ as the L^2 stratification error between the temperature field θ and the desired stratified field $S(y)$. The L^2 stratification errors and the L^2 norms of the velocity fields under different boundary conditions and Reynolds numbers are shown in Fig. 3. The evolution of the system can be divided into two stages: an initial stage where the L^2 stratification error stays almost the same, and a second stage where this error decays significantly.

The initial stage is shorter when the Reynolds number is larger (or the viscosity is smaller). According to Fig. 3[ab], the initial stage is up to $t = 600$ or more when $Re = 0.01$, and only up to $t = 1$ when $Re = 100$. In this stage, there is little or no stratification of the temperature field, as observed in the $Re = 0.01$ case in Fig. 2. Note the L^2 norms of the velocity decay sharply in a very short time window roughly from $t = 0$ to $t = 0.02$ for $Re = 1, 10, 100$ in Fig. 3[cd], where the decay is faster when the Reynolds number is smaller. This can be explained as follows. The removal of the temperature from the Boussinesq system results in a simple model: $\partial_t \mathbf{u} + \mathbf{u} \cdot \nabla \mathbf{u} = -\nabla p + \nu \Delta \mathbf{u}$ and $\nabla \cdot \mathbf{u} = 0$ on the square domain $\Omega = (-1,1)^2$ with either the slip or no-slip boundary condition. It is easy to derive the estimate $\|\mathbf{u}\|_{L^2(\Omega)}(t) \leq \|\mathbf{u}\|_{L^2(\Omega)}(0)e^{-\frac{ct}{Re}}$, where c is a constant only dependent on the domain. This suggests that the velocity's L^2 norm is smaller when Re is lower. We call the initial stage the "viscous dissipation stage" because it is the viscosity, not the stratification, that governs the velocity dissipation.

In the second stage, the system enters the stratification process. By fitting the asymptotic behavior observed in most simulations, we attain the following approximations,

$$\|\theta(x, y, t) - S(y)\|_{L^2(\Omega)} \approx \alpha \frac{1}{\sqrt{Re \cdot t}}, \tag{4.1}$$

$$\|\mathbf{u}\|_{L^2(\Omega)} \approx \frac{\beta}{Re^{0.24}t^{1.2}}. \tag{4.2}$$

For the simulations in this study, $\alpha_{slip} = 6$, $\alpha_{noslip} = 30$, $\beta_{slip} = 0.7$, and $\beta_{noslip} = 1.2$. These values are expected to vary depending on the initial conditions and domain configurations. From (4.1) and (4.2), we can derive

$$\|\mathbf{u}\|_{L^2(\Omega)} \approx \frac{\beta\sqrt{\|\theta(x, y, t) - S(y)\|_{L^2(\Omega)}}}{\sqrt{\alpha}\, t}. \tag{4.3}$$

Due to this direct relation between the velocity L^2 norm and the stratification error, we call this stage the "stratification stage".

Note the decay rates on time $t^{-0.5}$ in (4.1) and $t^{-1.2}$ in (4.2) are the same as those in Doering et al. (2018) in the corresponding norms. The formulas (4.1) and (4.2) along with the relations $\alpha_{slip} < \alpha_{noslip}$ and $\beta_{slip} < \beta_{noslip}$ show that the temperature stratification and velocity damping are more efficient under the larger Reynolds number and under the slip boundary condition. One possible explanation is that at higher Reynolds numbers (or under slip boundary conditions), less energy is lost to viscous dissipation (or boundary friction), allowing more kinetic energy from the initial stage to persist. This retained energy accelerates the stratification.

The stratification state $S(y)$ of the initial temperature in this work is a nonlinear function of the height (see Figure 1[b]). It is identical to the general temperature equilibrium $H(x_2)$ studied in Section 1.3. The L^2 norm of $\partial_t\mathbf{u}$, or $\|\partial_t\nabla\psi\|_{L^2(\Omega)}$ is plotted in Figure 4, which is bounded and almost proportional to the viscosity (or inversely proportional to Re) in the stratification stage. This partially verifies (1.15) in Theorem 1.2. The numerical result in Figure 4 also shows that $\|\partial_t\nabla\psi\|_{L^2(\Omega)}$ decays on time with order t^{-2} in the stratification stage, not given in Theorem 1.2. This warrants future research to address this gap.

4.2 Seesaw oscillations at Reynolds numbers

With $Re = 100$ and the slip boundary condition, amplitude-decaying oscillations are observed in both the L^2 stratification error (Figure 3[a]) and the L^2 norm of the velocity field (Figure 3[c]). The L^2 stratification error is also replotted on a linear scale in Fig. 5, revealing an oscillation period of approximately 3. Snapshots of the temperature fields from $t = 23$ to $t = 29$ are shown in Fig. 6, illustrating a seesaw-like spinning motion. For instance, the green layer separating the red and blue regions in the temperature field tilts to the left at $t = 23$ around its center, becomes roughly horizontal at $t = 25$, and rotates to the right at $t = 26$. It then flattens again at $t = 28$ before shifting left once more at $t = 29$. In particular, the temperature field at $t = 29$ closely resembles that at $t = 23$, with both exhibiting L^2 stratification errors located near the peaks of the oscillations. Similarly, the temperature fields

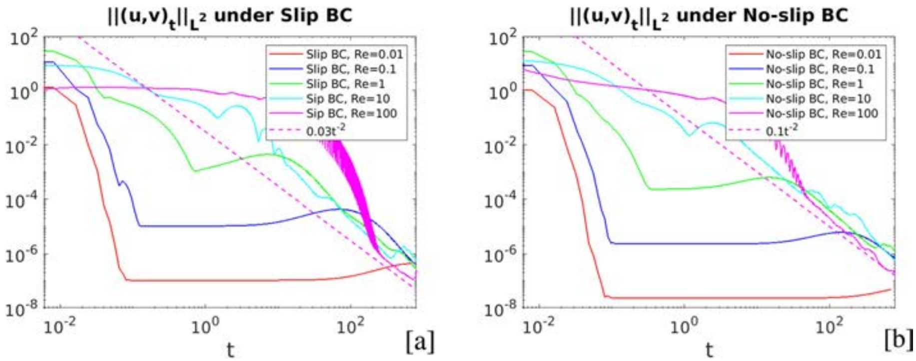

Fig. 4 $\|\partial_t \mathbf{u}\|_{L^2(\Omega)}$ under slip boundary condition **a** and no-slip boundary condition **b**

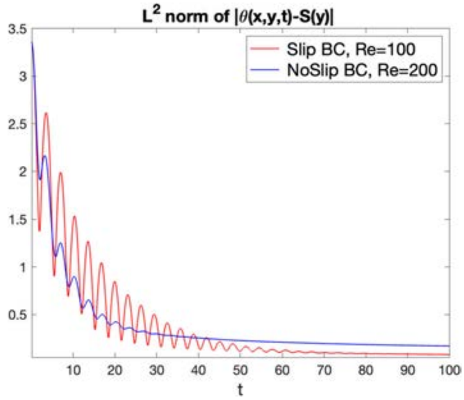

Fig. 5 L^2 norm of $|\theta(x, y, t) - S(y)|$ over time

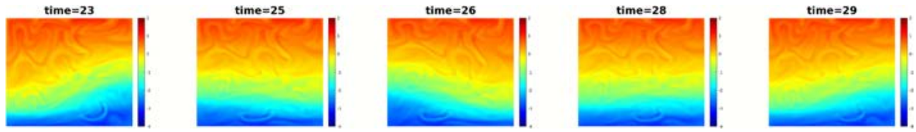

Fig. 6 Seesaw oscillations of the temperature fields from $t = 23$ to $t = 29$ under the slip boundary condition with $Re = 100$

at $t = 25$ and $t = 28$ are alike, and their corresponding L^2 stratification errors occur near the troughs.

The similar oscillations are also observed under the no-slip boundary condition but notably only with a larger Reynolds number such as $Re = 200$, whose snapshots are shown in Fig. 7. The oscillation amplitude is far smaller compared with that under the slip boundary condition when $Re = 100$ (see also Figure 5) but discernible by inspecting the direction of the mushroom in the bottom.

We call this process as seesaw oscillations because the green layer resembles a rigid seesaw oscillating repeatedly around the center. Because the seesaw rotation in the playground is driven by the gravity, we deduce this type oscillation in the temperature field is driven by the gravity/buoyancy force in this Boussinesq system. The seesaw motion is not present when the Reynolds number is small probably due to the strong viscous resistance, and it is also

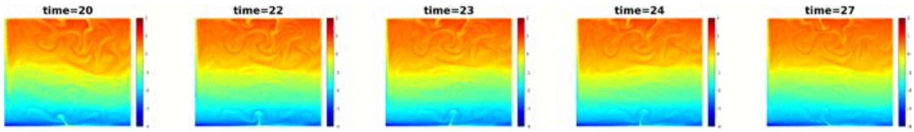

Fig. 7 Seesaw oscillations of the temperature fields from $t = 20$ to $t = 27$ under the no-slip boundary condition with $Re = 200$

difficult to appear under the no-slip boundary condition because of the boundary persistence mentioned in Section 4.1.1.

4.2.1 Interpretation of the seesaw oscillations

The seesaw motion can be inferred from the Fourier analysis in a special case. Here we cite some results from (Doering et al. 2018). The linearized system for the perturbation $\mathbf{U} = (U, V) = \mathbf{u} - \mathbf{u}_{he}$ with $\mathbf{u}_{he} = \mathbf{0}$, and $\Theta = \theta - S(y)$ is

$$\partial_t \mathbf{U} = \nu \Delta \mathbf{U} + \Theta \hat{\mathbf{e}}_2 - \nabla \Delta^{-1} \nabla \cdot (\Theta \hat{\mathbf{e}}_2), \tag{4.4}$$

$$\partial_t \Theta = -V S'(y). \tag{4.5}$$

In a special case where $S'(y) = \alpha$, a positive constant, the Fourier transform of the above system is

$$\frac{d}{dt}\begin{pmatrix} \widehat{U}_k \\ \widehat{V}_k \\ \widehat{\Theta}_k \end{pmatrix} = \begin{pmatrix} -\nu|k|^2 & 0 & -\frac{k_1 k_2}{|k|^2} \\ 0 & -\nu|k|^2 & \frac{k_2^1}{|k|^2} \\ 0 & -\alpha & 0 \end{pmatrix} \begin{pmatrix} \widehat{U}_k \\ \widehat{V}_k \\ \widehat{\Theta}_k \end{pmatrix}. \tag{4.6}$$

The eigenvalues of the coefficient matrix are $\lambda_1 = -\nu|k|^2$, $\lambda_{2,3} = \frac{1}{2}(-\nu|k|^2 \pm \sqrt{D})$ with $D = \nu^2|k|^4 - 4\alpha \frac{k_2^2}{|k|^2}$. When the Reynolds number is large (or the viscosity ν is small) such that $D < 0$, the solutions of $\widehat{U}_k$, $\widehat{V}_k$, $\widehat{\Theta}_k$ are in the form of

$$c_1 e^{-\nu|k|^2 t} + c_2 e^{-\nu|k|^2 t} \cos\left(\frac{\sqrt{|D|}}{2} t\right) + c_3 e^{-\nu|k|^2 t} \sin\left(\frac{\sqrt{|D|}}{2} t\right). \tag{4.7}$$

The sine and cosine functions in time can explain the oscillations in the convergence of the temperature and velocity fields over time when the Reunolds number is large.

5 Discussions and conclusions

The numerical simulations reveal that the evolution of the Boussinesq system in this study proceeds through two distinct stages. In the viscous dissipation stage, the flow is primarily governed by viscous effects, and the duration of this phase is shorter for the lower viscosity. In the subsequent stratification stage, the temperature field converges to the stratified state, where both the L^2 stratification error and the L^2 norm of the velocity decay following negative power laws in time and in the Reynolds number.

Furthermore, the numerical simulations indicate that temperature stratification occurs faster at higher Reynolds numbers, owing to reduced kinetic energy loss during the initial stage. On the other hand, stratification progresses slower under the no-slip boundary condition than under the slip condition, as boundary friction inhibits the flow dynamics. Notably, the no-slip boundary condition leads to more frequent boundary plume eruptions, which facilitates the stratification.

According to Theorem 1.1, the solution of the viscous Boussinesq system converges to that of the inviscid system in the limit of large Reynolds number under the slip boundary condition. The Reynolds number used in this work is between 0.01 and 200. To study the stratification of the inviscid Boussinesq system, it is fundamental to determine whether the L^2 stratification error (4.1) and the L^2 norm of the velocity (4.2) hold for all Reynolds numbers, and how the viscous dissipation stage and the seesaw oscillations evolve in the inviscid limit in the future work.

Acknowledgements J. Wu was partially supported by the National Science Foundation of the United States (Grant No. DMS 2104682 and DMS 2309748). X.Zheng was partially supported by NSF grant DMS-2309747. The three students E. Belayneh, X. Chen, and R. Nadam were supported by NSF grant DMS-2309747 to work on this research at Central Michigan University in Summer 2024. This work was supported in part by the computational resources and services provided by HPCC of the Institute for Cyber-Enabled Research at Michigan State University through a collaboration program of Central Michigan University.

Data Availability The data that support the findings of this study are available from the corresponding author upon reasonable request.

Declarations

Conflicts of Interest The authors declare that they have no conflict of interest.

References

Adhikari D, Ben Said O, Pandey U, Wu J, Stability and large-time behavior for the 2D Boussinesq system with horizontal dissipation and vertical thermal diffusion, *NoDEA Nonlinear Differential Equations Appl.* **29** (2022), no. 4, Paper No. 42, 43 pp

Bartello P, Tobias SM (2013) Sensitivity of stratified turbulence to the buoyancy Reynolds number. J Fluid Mech 725:1–22

Ben Said O, Pandey UR, Wu J (2022) The stabilizing effect of the temperature on buoyancy-driven fluids. Indiana Univ Math J 71(6):2605–2645

Bona JL, Wu J (2002) The Zero-Viscosity Limit of the 2D Navier-Stokes Equations. Stud Applied Math 109:265–278

Cheng J, Ji R, Tian L, Wu J (2025) Stability and enhanced decay rate for 3D anisotropic Boussinesq equations near the hydrostatic balance. J Differential Equations 425:300–341

Constantin P, Elgindi T, Ignatova M, Vicol V (2017) Remarks on the inviscid limit for the Navier-Stokes equations for uniformly bounded velocity fields. SIAM J Math Anal 49:1932–1946

Constantin P, Kukavica I, Vicol V (2015) On the Inviscid Limit of the Navier-Stokes Equations. Proceedings of AMS 143:3075–3090

Constantin P, Wu J (1995) Inviscid limit for vortex patches. Nonlinearity 8:735–742

de Bruyn Kops SM (2015) Classical turbulence scaling and intermittency in stably stratified Boussinesq turbulence. J Fluid Mech 775:436–463

Dong B, Wu J, Xu X, Zhu N (2021) Stability and exponential decay for the 2D anisotropic Boussinesq equations with horizontal dissipation, *Calc. Var. Partial Differential Equations* **60** , No.3, Paper No. 116, 21 pp
Doering C, Wu J, Zhao K, Zheng X (2018) Long time behavior of the two-dimensional Boussinesq equations without buoyancy diffusion. Physica D 376(377):144–159
Gie G, Kelliher JP, Lopes Filho M, Mazzucato AL, Nussenzveig Lopes H (2019) The vanishing viscosity limit for some symmetric flows, *Ann. Inst. H. Poincaré C Anal. Non Linéaire* **36** , 1237-1280
Holton JR, Hakim GJ (2012) An Introduction to Dynamic Meteorology (5th ed.), Academic Press,
Hu W, Wang Y, Wu J, Xiao B, Yuan Y (2018) Partially dissipative 2D Boussinesq equations with Navier-type boundary conditions. Physica D 376–377:39–48
Ji R, Yan L, Wu J (2022) Optimal decay for the 3D anisotropic Boussinesq equations near the hydrostatic balance. *Calc. Var. Partial Differential Equations* **61** , no. 4, Paper No. 136
Jiu Q, Niu D, Wu J (2012) Vanishing viscosity limits for the degenerate lake equations with Navier boundary conditions. Nonlinearity 25:641–655
Kukavica I, Vicol V, Wang F (2020) The inviscid limit for the Navier-Stokes equations with data analytic only near the boundary. Arch Ration Mech Anal 237:779–827
Kukavica I, Vicol V, Wang F (2022) Remarks on the inviscid limit problem for the Navier-Stokes equations. Pure Appl Funct Anal 7(1):283–306
Kukavica I, Wang W (2020) Long time behavior of solutions to the 2D Boussinesq equations with zero diffusivity. J Dynam Differential Equations 32(4):2061–2077
Lacave C, Mazzucato AL (2016) The vanishing viscosity limit in the presence of a porous medium. Math Ann 365:1527–1557
Lai S, Wu J, Xu X, Zhang J, Zhong Y (2021) Optimal decay estimates for the 2D Boussinesq equations with partial dissipation, *J. Nonlinear Science* **31** , No.1, 16
Laval JP, McWilliams JC, Dubrulle B (2003) 2003 Forced stratified turbulence: successive transitions with Reynolds number. Phys Rev E 68:036308
Pedlosky J (1987) *Geophysical Fluid Dynamics*, Springer,
Salmon R (1998) *Lectures on Geophysical Fluid Dynamics*, Oxford University Press,
Stefanov A, Wu J, Xu X, Ye Z (2025) Global regularity results of the 2D fractional Boussinesq equations. Math Ann 391(4):5965–6012
Tao L, Wu J, Zhao K, Zheng X (2020) Stability near hydrostatic equilibrium to the 2D Boussinesq equations without thermal diffusion. Arch Ration Mech Anal 237:585–630
Vallis GK (2017) Atmospheric and Oceanic Fluid Dynamics: Fundamentals and Large-Scale Circulation (2nd ed.), Cambridge University Press,
Wang W (2021) On the global solutions for the Boussinesq equations with Navier boundary conditions. Arch Math (Basel) 116(4):445–456
Wang W, Yue H (2020) Almost sure existence of global weak solutions to the Boussinesq equations. Dyn Partial Differ Equ 17(2):165–183
Wu J (2012) *The 2D Incompressible Boussinesq Equations*, Peking University Summer School Lecture Notes,
Wu J, Zhao K (2023) On 2D incompressible Boussinesq systems: global stabilization under dynamic boundary conditions. J Differential Equations 367:246–289
Zhou Q, Diamessis PJ (2016) Reynolds number effects in stratified turbulent wakes, In Proceedings of the 8th International Symposium on Stratified Flows, San Diego, CA,